Eur. Phys. J. Plus (2023) 138:419
https://doi.org/10.1140/epjp/s13360-023-04071-5

THE EUROPEAN PHYSICAL JOURNAL PLUS

Regular Article

Design of a compact long counter with an improved response using multiple point-like thermal neutron counters

Pengxiang Wang[1], **Zhimeng Hu**[1,2,a], **Xucheng Ma**[1], **Pin Gong**[1,2], **Guoqiang Zhong**[3], **Giuseppe Gorini**[4], **Baolong Chen**[5], **Xiaobin Tang**[1,2,b]

[1] Department of Nuclear Science and Technology, Nanjing University of Aeronautics and Astronautics, Nanjing 210016, China
[2] Key Laboratory of Nuclear Technology Application and Radiation Protection in Astronautics, Ministry of Industry and Information Technology, Nanjing University of Aeronautics and Astronautics, Nanjing 211106, China
[3] Institute of Plasma Physics, Chinese Academy of Sciences, Hefei 230031, China
[4] Department of Physics, University of Milan-Bicocca, 20126 Milan, Italy
[5] Nuclear and Radiation Safety Center, Ministry of Ecology and Environment, Beijing 100082, China

Received: 26 March 2023 / Accepted: 6 May 2023

Abstract A long counter with multiple point-like thermal neutron counters positioned in a cylindrical neutron moderator was investigated to improve the performance of the long counter, including flatter fluence response in a wider neutron energy range and also the compactness. The summation of the weighted counts of each thermal neutron counter yields the response of the long counter. In this study, silicon carbide (SiC) coated with ^{6}LiF convertor was used as the thermal neutron counter. In a further effort to balance the performance and structural complexity of long counters with multiple thermal neutron counters, the number and positions of these counters were first studied and optimized. As a result, the long counter with four specially positioned SiC counters showed the best performance. Besides, we also implemented a copper annular into the moderator to compensate for the long counter's response above a few MeV. The response function was relatively flat in the energy range from 10 eV to 25 MeV, with a relative standard deviation of approximately 1.78%. In addition, the proposed detector can evaluate the neutron energy, allowing it to monitor neutron fluence and neutron energy simultaneously.

1 Introduction

Neutron detectors that show "flat" energy dependence of the fluence response or H*(10) response over a wide energy range are recommended by the International Atomic Energy Agency (IAEA) to be used as transfer instruments for establishing neutron calibrations at Secondary Standards Dosimetry Laboratories. This type of detector could determine neutron fluence or ambient dose equivalent without using the information on a neutron spectrum and thus can serve usefully as a secondary standard instrument for traceability to the national standard. The method to avoid the difficulties in determining the total number of neutrons with heterogeneous energies was first proposed by Fermi and Amaldi [1]. They thermalized the neutrons of all energies in a large water tank and then integrated the thermal neutron density with respect to the distance from the source to obtain the total number of neutrons.

Inspired by Fermi and Amaldi's method, Hanson and Mckibben found that the counting rate of a long boron counter in a slab of paraffin is kind of independent of the incident neutron energy in a certain energy range [2]. Hence, they further had its paraffin moderator structurally designed to give a flat response function from 10 keV up to 3 MeV and named it a long counter. After Hanson and Mckibben's initial suggestion of such a neutron detector, various studies concentrated on enhancing the moderator design of the long counter for its advantages of high detection efficiency, insensitivity to gamma rays, reasonable directionality, and long-term stability [3–13].

Instead of employing a moderator with a complex structure, some studies merely used a polyethylene cylinder as the moderator and realized the flat response by changing the thermal neutron counters. One of them optimized the pressures and positions of two small spherical ^{3}He proportional counters in a polyethylene moderator so that their response functions peaking in two different energy intervals can be combined into a flat response function [14]. While the other study used a ^{3}He position-sensitive proportional counter divided into 20 regions to record the thermal neutrons' distribution along the axis of a polyethylene cylinder, and the distribution of neutron detection position was weighted before being summed up to realize the flat response [15]. What both studies

[a] e-mail: huzhm21@nuaa.edu.cn (corresponding author)
[b] e-mail: tangxiaobin@nuaa.edu.cn (corresponding author)

Published online: 18 May 2023

have in common is that they unevenly combined the counts of thermal neutron counters positioned at different depths in a moderator. As a result, the energy-independent fluence response function can be created by the linear combination of response functions that peak in different energy intervals.

However, the long counters designed by combining the counts of different thermal neutron counters are still relatively preliminary and their flat fluence response has yet to be perfected. Firstly, the response functions of the spherical ^{3}He proportional counter have only been calculated at limited positions in the moderator, and two of them were subjectively combined into a basically flat response function. By contrast, for the long counter using a ^{3}He position-sensitive proportional counter divided into 20 regions, the indiscriminate use of all 20 response functions seems to introduce unnecessary complexity.

In this study, we modeled 20 thermal neutron counters in a polyethylene cylinder to provide response functions at enough positions and discriminately used them in the linear combination. An objective process was described and used to determine the linear combination coefficients of the thermal neutron counters. We thereafter investigated how the combined flat response function varies with the number and position of the thermal neutron counters in use. Finally, by using four specifically positioned counters and copper for response compensation, a compact long counter with a flatter response function can be designed. Meanwhile, given a response matrix that is comparable to that of the Bonner sphere spectrometer (BSS) [16, 17], the detector also has a specific role in monitoring neutron fluence and neutron energy simultaneously.

2 Materials and methods

To obtain a flatter response function, it makes sense to utilize a set of response functions peaking in different energy ranges just as the BSS. Several response functions selected from a typical response matrix of the BSS can be linearly combined into a rather flat response function. We positioned point-like thermal neutron counters along the axis of a cylindrical moderator to construct a neutron long counter and therefore obtained a response matrix that is comparable to that of a typical BSS [18–22]. As shown in Fig. 1, regarding the diameter of the BSS sphere that is sensitive to neutrons around 20 MeV, we used a polyethylene cylinder with a length and diameter of 30 cm as the moderator to obtain response functions that peak around 20 MeV. For the 20 counters shown in Fig. 1, we aimed to select and combine their response functions optimally. Thus, we need to solve a system of overdetermined equations to produce the flattest possible response for a certain response function combination and then find the optimally performed one from all possible combinations. Through such a procedure, we can determine the most critical response functions needed in the combination of the flat fluence response and thus simplify the structure of the long counter.

The Monte Carlo code is used to calculate the energy response of the SiC thermal neutron counters. In our design, the response function of the long counter depends on a combination of multi-counter outputs instead of a single ^{3}He or BF_3 tube recorded counts as in most long counters. However, the long counter design and calibration work conducted through the Monte Carlo simulation can be particularly inefficient because the detection efficiency of the LiF-coated SiC thermal neutron counter is about 1000 times lower than that of the ^{3}He or BF_3 proportional counter. To improve the efficiency of the simulation, we take a two-step method, first utilizing the Monte Carlo code to determine the fluence energy distribution surrounding the thermal neutron counters. Subsequently, the response $R(E_n)(cm^2)$, defined as the recorded charged particle counts per unit fluence of incident neutrons, can be numerically calculated using the following formula [23]:

$$R(E_n) = a_s \cdot N_{6_{Li}} \cdot c \sum_{i=1}^{N} \Phi(E_i) \cdot \mathrm{S}(E_i) \cdot \sigma_{n,t}(E_i), \tag{1}$$

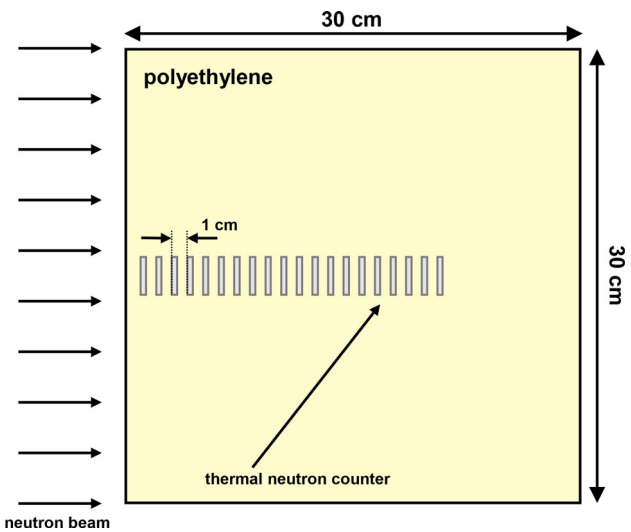

Fig. 1 Schematic geometry of the long counter

where E_n is the energy of the incident neutron energy, a_s is the parallel monoenergetic neutron beam area, N_{6Li} is the number of ^{6}Li atoms contained in the LiF convertor and c is the proportion of the number of ^{6}Li(n, t) reactions that the SiC counter recorded, which is determined by the solid angle of the SiC surface to the convertor assuming an isotropic angular distribution of the tritons produced. E_i is the midpoint of the i-th energy bin on the logarithmic coordinate axis, $\Phi(E_i)$ is the neutron fluence for neutrons in the i-th energy bin, $S(E_i)$ is the neutron self-shielding factor calculated assuming the plane detector model [24], and $\sigma_{n,t}(E_i)$ is the standard cross section obtained from the ENDF/B-VIII.0 Library [25] for ^{6}Li(n, t) interaction.

3 Results and discussion

3.1 Long counter with polyethylene moderator

3.1.1 Counter response in polyethylene moderator

As shown in Fig. 1, a total of 20 counter regions were modeled in 1 cm steps along the long axis of the cylindrical moderator for Monte Carlo simulations to calculate the response functions of these counters. The counter encapsulates a piece of SiC with a size of 5 mm*5 mm and thickness of 500 μm. A 5 μm LiF layer with a ^{6}Li enrichment of 90% was plated on its upper surface, and thus, a c value of 0.5 was used.

To determine the response functions of thermal neutron counters, a series of irradiation exposures were simulated, with parallel monoenergetic neutron beams of uniform density impinging perpendicularly on the front surface of the long counter. The energy of monoenergetic neutron beams covers neutron energies from thermal to 100 MeV, with 10 energies per decade. To model the thermal neutron scattering within the polyethylene moderator, the room temperature cross section S(α, β) tables were invoked based on the MT (poly.01 T) card, and the thermal neutron cross sections in original 1001.70c and replacement poly.01 T are shown in Fig. 2b. The responses were calculated at each of the 121 energy points using Eq. (1). Taking the response of the fifth thermal neutron counter in the left at 1keV incident neutrons as an example, the cross section $\sigma(E)$ for ^{6}Li(n, t), $S(E)$ for a LiF of 5 μm thickness, and the neutron fluence energy distribution $\Phi(E)$ surround it are shown in Fig. 2a. And as shown in Fig. 2c, the energy distribution of the recorded alphas and tritons in this counter was also simulated by irradiating the LiF-covered SiC using a parallel neutron beam the energy distribution of which is set according to $\Phi(E)$. Finally, the calculated response functions are shown as a response matrix in Fig. 3.

3.1.2 Determination of the linear combination coefficients

In this section, we intend to find a method that can linearly combine a set of response functions arbitrarily selected from Fig. 3 into the flattest possible response function in a certain energy range. Using such a method, we may assess the performance of any response function combination and then identify the optimally performed one from all possible combinations. Assuming we have arbitrarily chosen j response functions out of a total of 20, this linear combination can be expressed by the following equation:

$$R_{\text{ideal}} = \sum_j R_j \cdot w_j, \tag{2}$$

where R_j is the portion of the selected j-th response function within the expected energy-independent energy range, w_j is the coefficient corresponding to R_j, R_{ideal} is a constant function that represents the ideal flat response. We may further express the equation in a matrix form:

$$R_{\text{ideal}} = R \cdot w, \tag{3}$$

where R is an $i \times j$ coefficient matrix with i the number of energy points within the expected energy-independent energy range.

To deal with such an overdetermined set of equations without exact solutions, it makes sense to search for the vector w which is closest to being a solution, in the sense that to minimize the residual errors Δ between the ideal and combined responses given as

$$\Delta = \| R_{\text{ideal}} - Rw \|_2 = \sqrt{(R_{\text{ideal1}} - (Rw)_1)^2 + (R_{\text{ideal2}} - (Rw)_2)^2 + \ldots}. \tag{4}$$

This process implies finding the least squares solution of $Rw = R_{\text{ideal}}$, which is equivalent to solving the normal equation $R^T Rw = R^T R_{\text{ideal}}$, where $\mathrm{R^T}$ is the transpose matrix of R. Thus, the coefficient vector w found by the least squares method is

$$w = (R^T R)^{-1} R^T R_{\text{ideal}}. \tag{5}$$

3.1.3 Combined response function

To determine the optimal configuration of thermal neutron counters, we consider all possible combinations of 2 to 10 counters out of a total of 20. Using the method described above, we calculate the coefficient vector for each combination. For example,

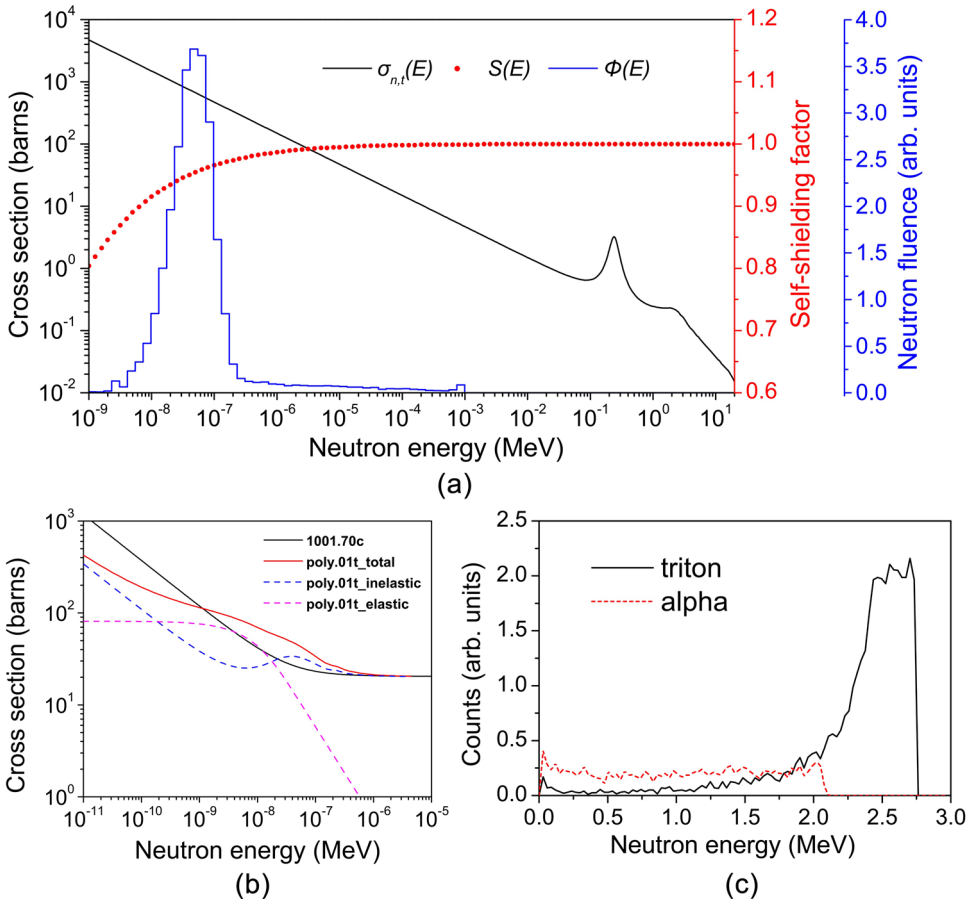

Fig. 2 **a** The cross section for ^{6}Li(n, t) reaction, self-shielding factor for a LiF of 5 μm thickness, and the neutron fluence energy distribution in the fifth tally cell from left to right facing the 1 keV neutron beam; **b** The thermal neutron cross sections for S(α, β) material polyethylene;**c** The energy distribution of the alphas and tritons entering the fifth thermal neutron counter from left to right facing the 1 keV neutron beam

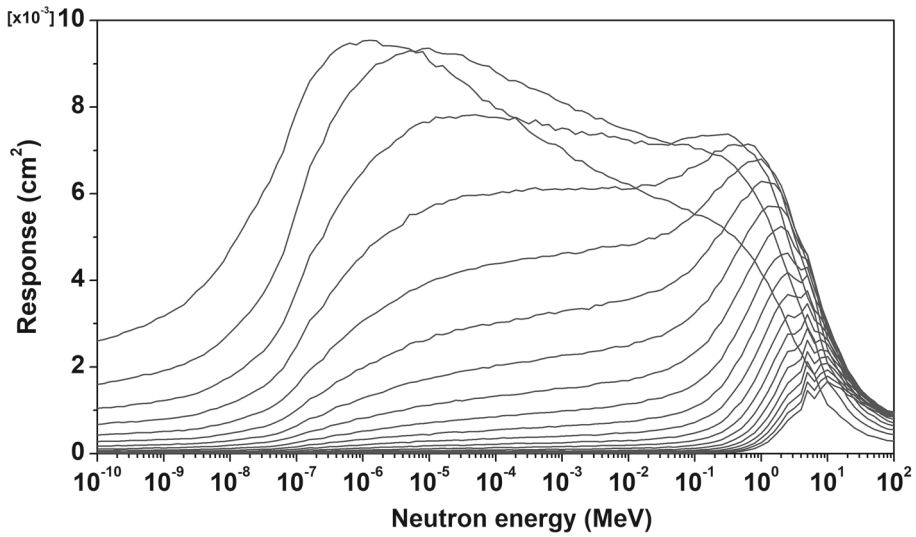

Fig. 3 Calculated response functions for the thermal neutron counters embedded in the polyethylene moderator. 20 curves from left to right correspond to 20 counter regions modeled in the moderator from the shallower to the deeper

when constructing a long counter with five counters, we compute the coefficient vectors for $C_{20}^{5} = \frac{20!}{5!\cdot 15!} = \frac{20\cdot 19\cdot 18\cdot 17\cdot 16}{5\cdot 4\cdot 3\cdot 2\cdot 1} = 15504$ combinations. Then, for each counter combination and its corresponding combined response function, we can calculate the relative standard deviation (RSD) of its responses in the planned energy-independent range and determine the combination with the minimum RSD. Figure 4 shows the minimum RSD for long counters constructed with various numbers of counters in different energy ranges.

The results show that, with more counters in use, the RSD of the response functions in these energy ranges initially decreases and then remains at a certain level. When the energy-independent energy range is set to 10 eV–5 MeV, using three counters is sufficient. If the upper energy limit is extended to 10, 15, and 20 MeV, or the lower energy limit is extended to 1 eV, using five counters is

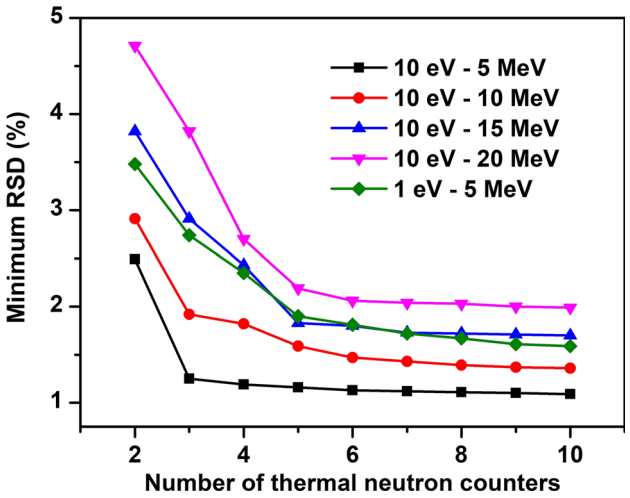

Fig. 4 Minimum RSDs of the long counters using various numbers of thermal neutron counters in different energy ranges

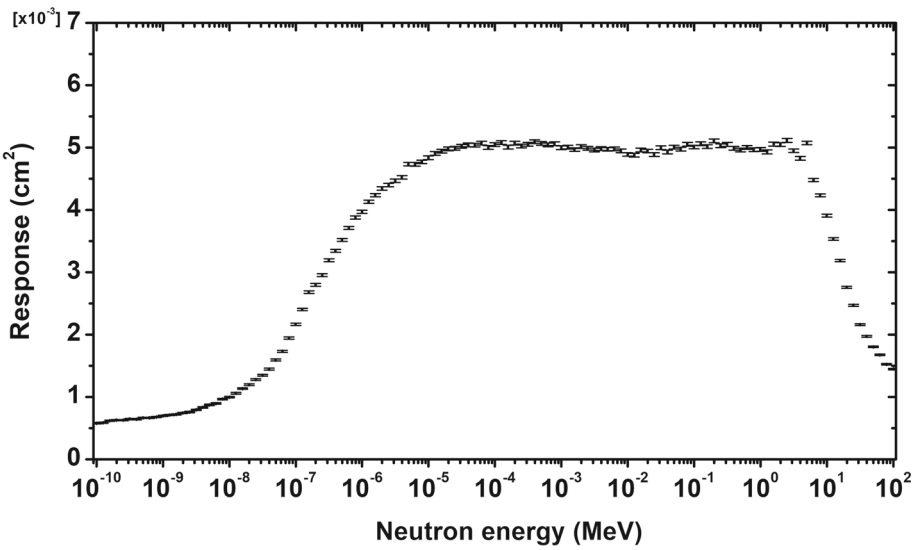

Fig. 5 Combined response function of the long counter with polyethylene moderator in the energy range from 10 eV to 5 MeV

appropriate. Beyond these points, adding more counters does not remarkably reduce the RSD of the response function, but only complicates the structure of the long counter.

We first plot the optimized linear combination in the energy range from 10 eV to 5 MeV. As shown in Fig. 5, the combined response function appears rather flat. To assess its flatness, we use the RSD in this study rather than the previously used maximum relative deviation to the mean because materials, such as polyethylene and cadmium, which are commonly used in the long counter design, have narrow resonances in their neutron cross sections. These resonances can considerably increase the maximum relative deviation and mask the overall flatness of the response function. Meanwhile, to exhibit the improvement of the linear combination to the flatness of the response function, the RSDs of the response functions for other long counters with polyethylene moderators are also calculated, as listed in Table 1. Given that their flat response functions span various energy ranges, the overlap of each two energy ranges was chosen to assess their flatness fairly. The terms RSD-1 and RSD-2 denote the RSDs of the flat response functions for the long counters in this study and previous research, respectively. The flat response function obtained in this work has a considerably smaller RSD than that of the other long counters. In addition to JAEA's compact long counter using polyethylene and polystyrene moderators, the long counter designed in this work is roughly half the weight of a typical long counter.

However, as shown in Fig. 6, when the upper energy limit is extended beyond 5 MeV, each of the responses above 5 MeV has a large error. This phenomenon occurs because the responses above 5 MeV depend entirely on the deep-positioned counters, but their responses are much smaller than that of the shallow-positioned counters, requiring rather large coefficients to raise them, resulting in larger errors. Additionally, the error and unevenness of the response function also slightly increase when the lower energy limit is extended to 1 eV. The error bar given in this study only considers the statistical error of the simulation results. Later in our experimental work on the actual construction of this long counter, a thorough analysis of the errors from many aspects, such as the counter or the moderator material, will be conducted [17, 26].

Table 1 Performance parameters of long counters with polyethylene moderator. RSD-1 and RSD-2 denote the RSDs of the response functions for the long counters in this study and previous research in their overlapping flat response energy range

Long counter	Flat response Energy range	Overlapping energy range	RSD-1 (%)	RSD-2	Moderator size	Weight	Thermal convertor	Average response
IRSN [5]	5 eV–2.5 MeV	10 eV–2.5 MeV	2.06	1.17%	Diameter 40 cm, length 40 cm	~50 kg	^{3}He	~10 cm^2
KIRSS [8]	1 keV–8 MeV	1 keV–5 MeV	5.13	1.20%	Diameter 41 cm, length 50 cm	~60 kg	^{3}He	~15 cm^2
JAEA [9]	0.4 keV–5 MeV	0.4 keV–5 MeV	5.10	1.25%	Diameter 22 cm, length 37 cm	~15 kg	^{3}He	–
This work	10 eV–5 MeV	–	1.16	–	Diameter 30 cm, length 30 cm	~20 kg	LiF	~0.005 cm^2

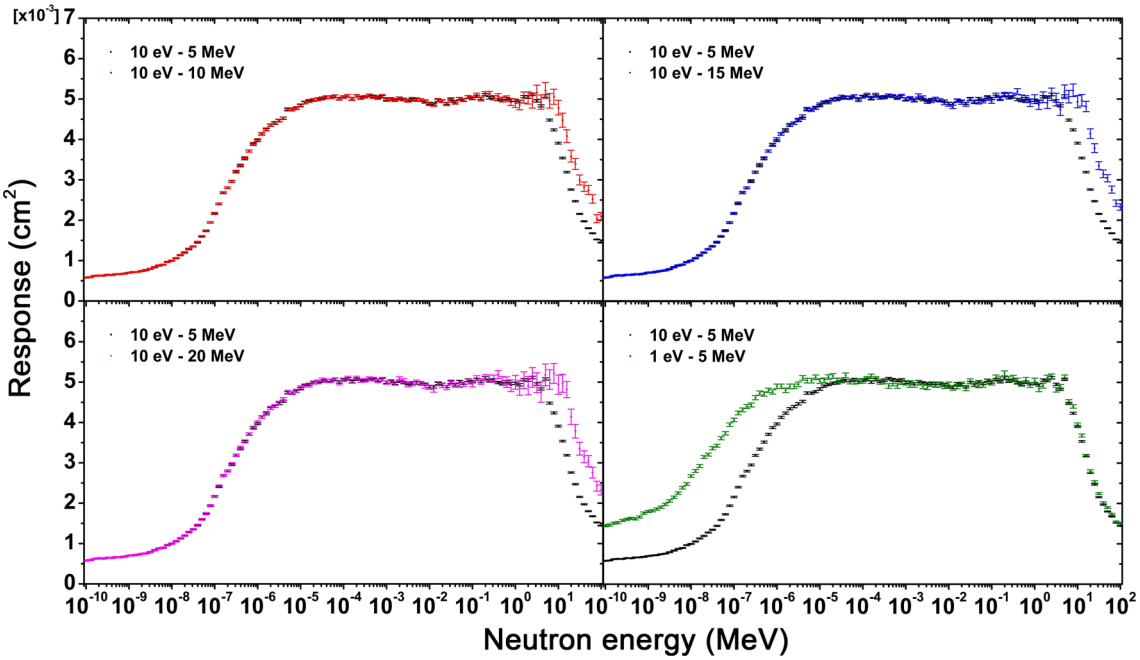

Fig. 6 Combined response functions of detectors with polyethylene moderators in different energy ranges

3.2 Long counter with response compensation

To reduce the error of the responses above 5 MeV, the counter response can be enhanced by incorporating metal materials with a higher atomic number. As is the case with other response-compensated neutron detectors, high-energy neutrons can be converted into multiple low-energy neutrons through the (n, xn) reaction. In previous design work on response-compensated long counters, various metal materials were evaluated. On the basis of these results, we selected copper due to its relatively flat response in the high-energy range [13, 27], and the cross sections for Cu(n, xn) from ENDFB-VIII.0 library [25] are shown in Fig. 7.

A copper annulus with an inner diameter of 10 cm and a length of 13 cm was embedded in the moderator, and a 10-cm-long air annulus was set in front of it. Initial simulations used a 2-cm-thick copper annulus, but the response functions exhibited jagged peaks that could not be integrated into a flat response function due to the resonance of the copper's neutron cross section. Subsequent simulations with a 1-cm-thick copper annulus can obtain flat combined response functions in five energy ranges through the same procedure described above.

As shown in Fig. 8, the embedded copper annulus effectively reduces the error of the responses above 5 MeV. The flat response function with the upper energy limit extended to 30 MeV still has a small error. However, the response at 30 MeV in this curve is considerably lower than the curve's overall flat response, indicating that the upper energy limit of the flat response function cannot be raised to 30 MeV or higher with this design. Additionally, when the lower energy limit is extended to 1 eV, the error and unevenness of the response function increase. Therefore, with this long counter design, combining the response functions in the 10 eV–25 MeV energy range is relatively appropriate. In subsequent simulations, we set the inner diameter of the copper annulus to 8, 10, and 12 cm

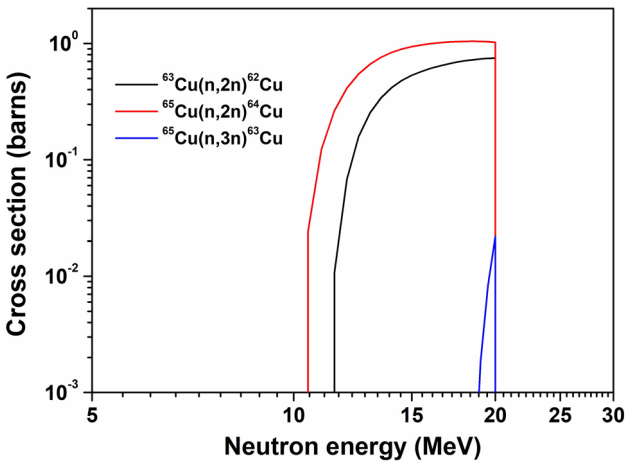

Fig. 7 The graph of neutron cross section for Cu(n, xn) from ENDFB-VIII.0 library

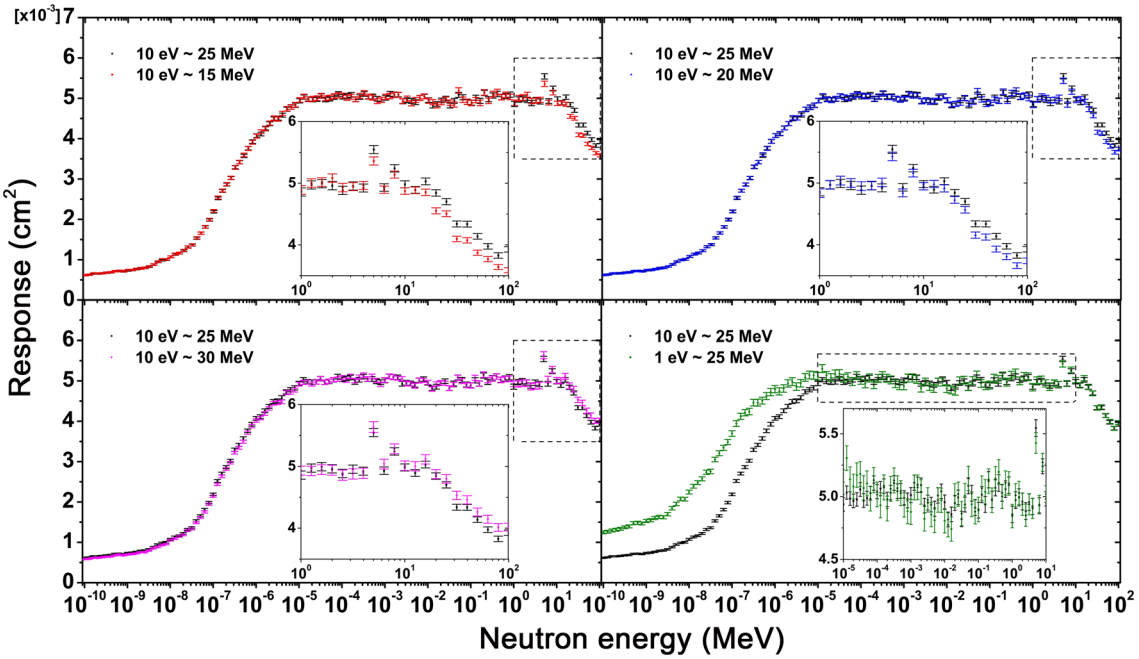

Fig. 8 Combined response functions of detectors with response compensation in different energy ranges

and the length of the air annulus to 5, 10, and 15 cm to calculate the response function and combined nine response functions as shown in Fig. 9.

The results reveal that the three response functions in the right-hand column exhibit larger deviations compared with the other response functions, and their geometrical designs are not suitable. For the remaining six response functions, five of them have one or two responses that are offset from the mean. Only the design with an inner diameter of 8 cm for the copper annulus and a length of 5 cm for the air annulus corresponds to a response function with no responses that are offset from the mean, which is the appropriate geometrical design. Given that long counters usually operate in environments with scattered neutrons, 1-cm-thick borated polyethylene is inserted in the side and back to ensure the directional response. The final schematic geometry of the long counter is shown in Fig. 10.

We also assessed its flatness with RSD and compared it with those of other response-compensated long counters in the overlapping energy ranges. As listed in Table 2, the long counter designed in this work has the smallest RSD and the lightest weight. Its response function is flatter over a wider energy range than that of the FDS-1. Moreover, for the long counters with the flat response energy range further extended, the linear combination method could be involved to reduce their RSDs. In addition, to evaluate the effect on RSD due to different flat response energy ranges and various compensator geometries, the RSD values for the response functions shown in Figs. 6, 8, and 9 are listed in Table 3. Finally, our design with thin-film coated SiC counter at this stage surely needs a rather long time to attain reasonable statistics, but the improvement of the detection efficiency of compact diode detectors has long been of interest and schemes such as etching micro-trench or micro-perforation on the diode surface have been proposed [28, 29].

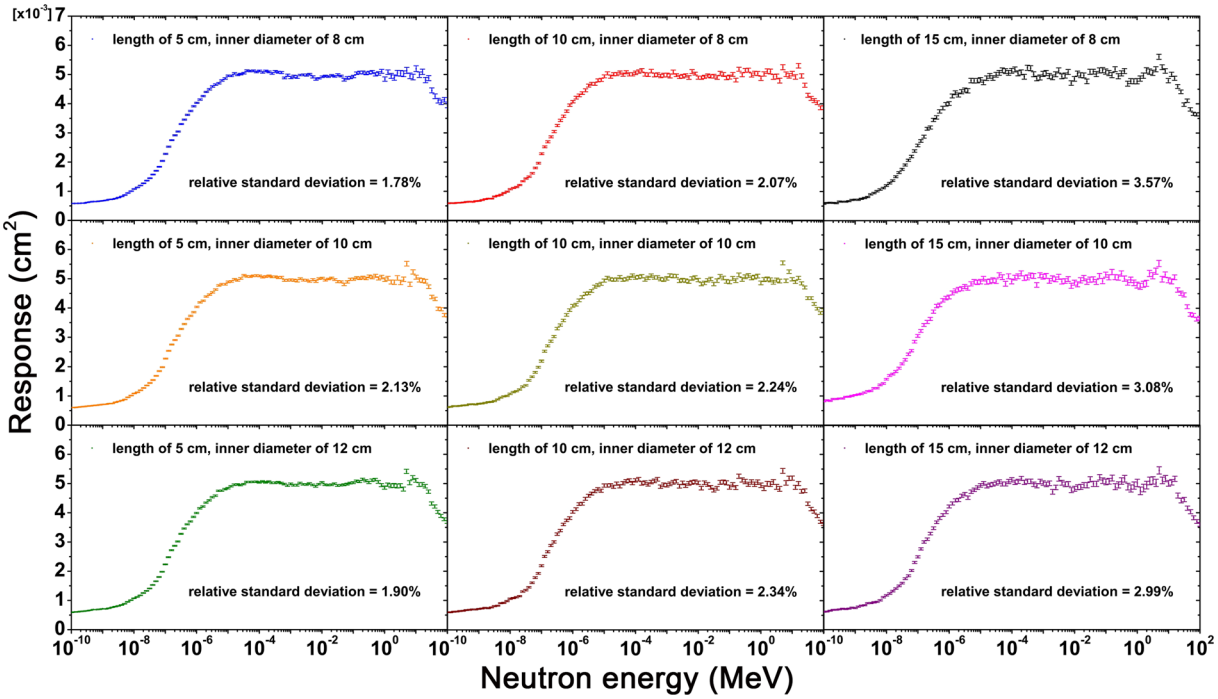

Fig. 9 Combined response functions for nine geometrical designs

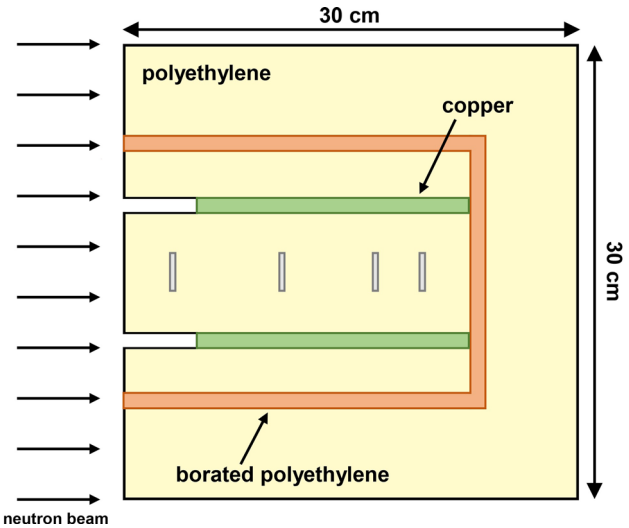

Fig. 10 Final schematic geometry of the long counter

By adopting this kind of microstructured semiconductor neutron detector, the average response of our long counter can hopefully reach 0.1 cm^2 or higher.

3.3 Effective center of the long counter

For a typical long counter, the effective center is located on the axis of the cylindrical moderator, r_0 from the front surface. Assuming such an exact position, the long counter's count rate from a point source is inversely proportional to $(r + r_0)^2$, where r is the distance from the source to the front face of the long counter.

For the long counter designed in this work, we first ensure that combining the counts of different counters does not interfere with the determination of physically relevant effective centers. In accordance with the standard effective center determination procedure, several monoenergetic point sources are used to evaluate the effective center of this long counter [30]. Monte Carlo simulations are conducted at 20 distances between the source and the long counter's front surface ranging from 120 to 500 cm, considering intervals of 20 cm.

Table 2 Performance parameters of long counters with response compensation. RSD-1 and RSD-2 denote the RSDs of the response functions for the long counters in this study and previous research in their overlapping flat response energy range

Long counter	Flat response Energy range	Overlapping energy range	RSD-1 (%)	RSD-2	Moderator size	Weight	Thermal convertor	Average response
FDS-1 [10]	1 keV–20 MeV	1 keV–20 MeV	2.83	1.74%	Diameter 30 cm, length 37 cm	~35 kg	^{3}He	~0.3 cm^2
FDS-2 [11]	0.1 keV–150 MeV	0.1 keV–25 MeV	4.32	1.80%	Diameter 40 cm, length 46 cm	~65 kg	^{3}He	~1.2 cm^2
FDS-3 [13]	1 eV–800 MeV	10 eV–25 MeV	7.11	1.78%	Diameter 50 cm, length 50 cm	~100 kg	BF_3	~1 cm^2
This work	10 eV–25 MeV	–	1.78	–	Diameter 30 cm, length 30 cm	~25 kg	LiF	~0.005 cm^2

Table 3 The RSD values for the response functions shown in Figs. 6, 8, and 9

Flat response Energy range	Inner diameter of copper annulus	Length of air annulus	RSD
1 eV–5 MeV	Without compensation		1.90%
10 eV–5 MeV	Without compensation		1.30%
10 eV–10 MeV	Without compensation		1.69%
10 eV–15 MeV	Without compensation		1.91%
	10 cm	10 cm	1.90%
10 eV–20 MeV	Without compensation		2.50%
	10 cm	10 cm	2.08%
1 eV–25 MeV	10 cm	10 cm	3.38%
10 eV–25 MeV	8 cm	5 cm	1.78%
		10 cm	2.07%
		15 cm	3.57%
	10 cm	5 cm	2.13%
		10 cm	2.24%
		15 cm	3.08%
	12 cm	5 cm	1.90%
		10 cm	2.34%
		15 cm	2.99%
10 eV–30 MeV	10 cm	10 cm	2.66%

Figure 11a shows the simulation results for the neutron energy at 0.144 MeV. For each of the 20 different source-to-detector distances, six separate simulations are conducted with six different pseudorandom numbers, and the result is averaged over the six runs [31]. r_0 is determined to be 2.86 cm for the neutron energy at 0.144 MeV, and the effective centers determined for the remaining neutron energies are shown in Fig. 11b.

3.4 Energy measuring capability

In this work, the flat response function is built on a response matrix that is comparable with a typical BSS response matrix, that is, such a detector also has the potential to measure neutron energy. For this purpose, we selected the essential response functions in the response matrix to maintain its energy-measuring capacity. The selection of response functions and evaluation of the energy measuring capacity is conducted using a widely accepted resolving power determining procedure. It is proposed by Reginatto with reference to a procedure proposed in the context of geophysical inverse problems [32]. This method considers the linear average of the neutron spectrum $\Phi(E)$ at an energy point E_0 using average kernel $A(E_0, E)$ as closely as feasible to the Dirac delta function:

$$\langle \Phi \rangle_{E_0} = \int A(E_0, E)\Phi(E)dE. \tag{6}$$

To quantify the energy resolution with the average kernel, the following two parameters are presented:

$$L_{AV}(E_0) = \int A(E_0, E)EdE. \tag{7}$$

$$[\Delta L(E_0)]^2 = \int A(E_0, E)(E - L_{AV}(E_0))^2 dE. \tag{8}$$

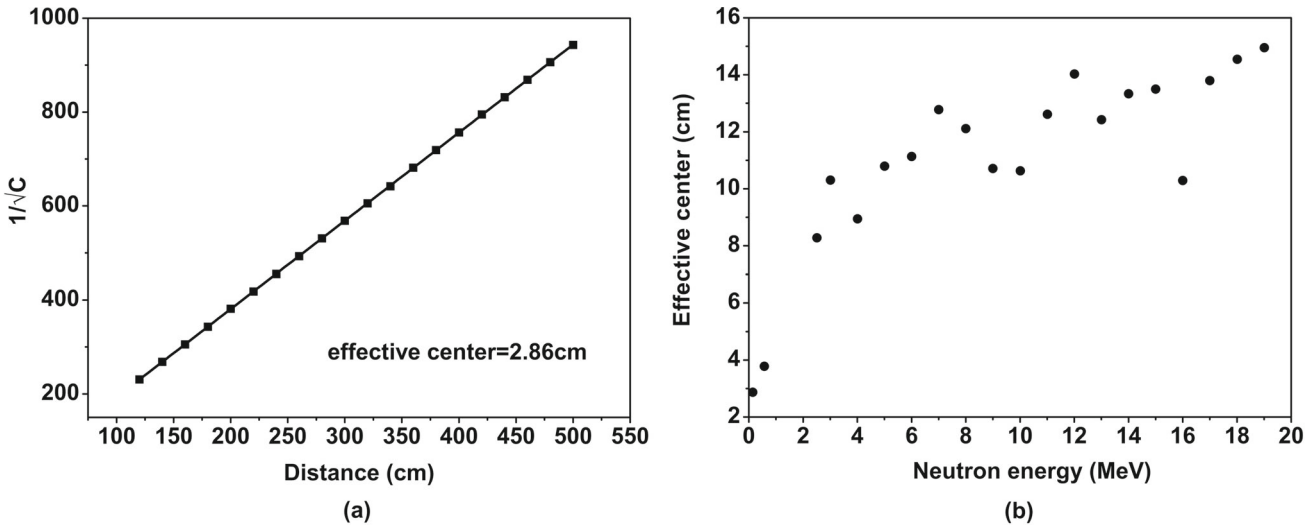

Fig. 11 Calculation result of effective center. **a** Effective center obtained from linear fitting against distances from a 0.144 MeV neutron source to the front face of the long counter. **b** Effective centers calculated at several neutron energies

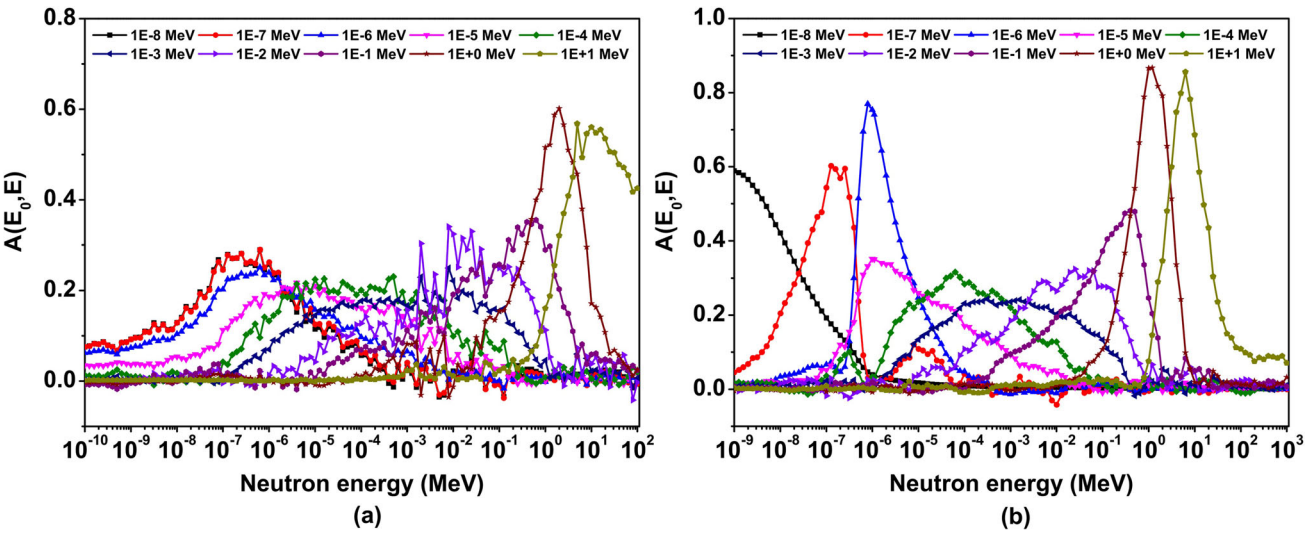

Fig. 12 Averaging kernels $A(E_0, E)$ of **a** the long counter designed in this work and **b** the PTB BSS

The breadth of the averaging kernel $A(E_0, E)$ is measured by parameter $\Delta L(E_0)$, whereas parameter $L_{AV}(E_0)$ measures how accurately the averaging kernel is centered on E_0. If $L_{AV}(E_0) \rightarrow E_0$ and $\Delta L(E_0) \rightarrow 0$, it indicates that the averaging kernel provides a good approximation to a delta function and the spectrometer features a good energy resolution. Finally, in addition to the four sensors used for the long counter, two additional sensors were needed to maintain its energy measurement capability.

As shown in Fig. 12a and b, its performance as a BSS is evaluated against the PTB BSS [17]. In general, constrained by the number of detectors in use, its energy resolution is worse than that of the PTB BSS. Especially in the low-energy range, the averaging kernels of 10^{-8} MeV and 10^{-7} MeV nearly overlap with each other because there is no response function in the response matrix peaks at 10^{-8} MeV. However, as the energy increases to keV or higher, as given in Table 4, $L_{AV}(E_0)$ is relatively concentrated around E_0, $\Delta L(E_0)$ is gradually reduced, and the averaging kernels demonstrate a similar shape and variation pattern as that of the PTB BSS.

Table 4 Averaging kernel parameters

$\log_{10}$(E/MeV)	PTB − L_{AV}	L_{AV}	PTB − ΔL	ΔL
− 8	− 7.72	− 6.30	1.86	3.85
− 7	− 6.34	− 6.40	1.94	3.20
− 6	− 5.72	− 6.04	1.14	3.87
− 5	− 4.92	− 5.02	2.44	4.76
− 4	− 3.92	− 3.97	2.36	3.78
− 3	− 3.02	− 3.10	2.87	3.33
− 2	− 2.06	− 2.11	2.53	2.68
− 1	− 1.12	− 1.14	1.82	1.78
0	− 0.07	− 0.18	0.78	1.35
+ 1	0.84	0.77	1.12	1.53

4 Conclusion

In this study, we analyzed the number and positions of the thermal neutron counters embedded in the cylindrical neutron moderator of the long counter to optimize its response flatness in a wider neutron energy range and simplify its structure. As a result, a compact long counter with four specially positioned SiC thermal neutron counters was designed and evaluated. The long counter is 30 cm in diameter and 30 cm in length, and only one-half in weight of a typical long counter. After response combination and compensation, its response function can be rather flat in the energy range of 10 eV to 25 MeV, with an RSD of 1.78%. Additionally, the proposed detector features flat response and energy measuring ability, which is verified by comparing it with the PTB BSS through a commonly accepted procedure.

In future works, we will experimentally construct this long counter following the above design. The response function and effective centers of the long counter will be carefully calibrated by combining the Monte Carlo simulations and measurements in the reference neutron fields. After the experimental characterization, in consideration of the low detection efficiency of the SiC thermal neutron detector, neutron fluence measurements with this long counter may be conducted further in the high-density neutron field of the Experimental Advanced Superconducting Tokamak.

Acknowledgements This work was finically supported by the National Natural Science Foundation of China (No. 12105144), China Postdoctoral Science Foundation (No. 2022M721659), the Primary Research and Development Plan of Jiangsu Province (Grant No. BE2022846), the Fundamental Research Funds for the Central Universities (Grant No. NC2022006), and the Foundation of Graduate Innovation Center in NUAA (Grant No. xcxjh20220607).

Data Availability Statement This manuscript has associated data in a data repository. [Authors' comment: Data will be made available upon reasonable request.]

References

1. E. Amaldi, L.R. Hafstad, M.A. Tuve, Neutron yields from artificial sources. Phys. Rev. **51**(11), 896 (1937). https://doi.org/10.1103/PhysRev.51.896
2. A.O. Hanson, J.L. McKibben, A neutron detector having uniform sensitivity from 10 keV to 3 MeV. Phys. Rev. **72**(8), 673 (1947). https://doi.org/10.1103/PhysRev.72.673
3. J. De Pangher, L.L. Nichols, A Precision long counter for measuring fast neutron flux density, BNWL-260. Pacific Northwest Laboratory (1966)
4. H. Tagziria, D.J. Thomas, Calibration and monte carlo modelling of neutron long counters. Nucl. Instrum. Methods Phys. Res. A **452**(3), 470–483 (2000). https://doi.org/10.1016/S0168-9002(00)00448-4
5. V. Lacoste, Design of a new long counter for the determination of the neutron fluence reference values at the IRSN AMANDE facility. Radiat. Meas. **45**(10), 1250–1253 (2010). https://doi.org/10.1016/j.radmeas.2010.06.026
6. V. Lacoste, V. Gressier, Experimental characterization of the IRSN long counter for the determination of the neutron fluence reference values at the AMANDE facility. Radiat. Meas. **45**(10), 1254–1257 (2010). https://doi.org/10.1016/j.radmeas.2010.07.004
7. G.D. Kim, H.J. Woo, J.H. Park, T. Yoshihiko, Y. Michio, Characteristics of the KIGAM long-counter for the neutron energy range below 2.5 MeV. J. Korean Phys. Soc. **61**, 347–352 (2012). https://doi.org/10.3938/jkps.61.347
8. H. Park, J. Kim, K.O. Choi, Long counter and its application for the calibration of the neutron irradiators. Radiat. Prot. Dosim. **161**(1–4), 161–165 (2014). https://doi.org/10.1093/rpd/nct351
9. Y. Tanimura, M. Tsutsumi, M. Yoshizawa, Development of portable long counter with two different moderator materials. Radiat. Prot. Dosim. **161**(1–4), 144–148 (2014). https://doi.org/10.1093/rpd/nct345
10. Y. Li, T. Li, G. Song, M. Mazunga, FDS Team, Response improved for neutron long counter. Radiat. Prot. Dosim. 164(1-2), 93–96 (2015). https://doi.org/10.1093/rpd/ncu348
11. M. Mazunga, T. Li, Y. Li, B. Hong, Y. Wang, X. Ji, Design of an extended range long counter using super Monte Carlo simulation. Radiat. Prot. Dosim. **175**(3), 413–417 (2017). https://doi.org/10.1093/rpd/ncw368
12. B. Hong, C. Liu, T. Li, Y. Wang, Y. Li, M. Mazunga, Calibrations of the FDS long counter for neutron fluence measurement. Nucl. Technol. **201**(2), 174–179 (2018). https://doi.org/10.1080/00295450.2017.1406270
13. Y. Li, T. Li, H. Guo, Y. Wang, Improvements to the long counter for neutron energies up to GeV. Radiat. Meas. **140**, 106504 (2021). https://doi.org/10.1016/j.radmeas.2020.106504

14. H. Harano, T. Matsumoto, J. Nishiyama, A. Masuda, A. Uritani, K. Kudo, Development of a compact flat response neutron detector. IEEE Trans. Nucl. Sci. **58**(5), 2421–2425 (2011). https://doi.org/10.1109/TNS.2011.2163191
15. K. Watanabe, J. Otsuka, M. Shigeyama, Y. Suzuki, A. Yamazaki, A. Unitani, Flat-response neutron detector using spatial distribution of thermal neutrons in a moderator. Nucl. Instrum. Methods Phys. Res. A **652**(1), 392–396 (2011). https://doi.org/10.1016/j.nima.2010.08.044
16. R.L. Bramblett, R.I. Ewing, T.W. Bonner, A new type of neutron spectrometer. Nucl. Instrum. Methods **9**(1), 1–12 (1960). https://doi.org/10.1016/0029-554X(60)90043-4
17. A.V. Alevra, D.J. Thomas, Neutron spectrometry in mixed fields: multisphere spectrometers. Radiat. Prot. Dosim. **107**(1–3), 33–68 (2003). https://doi.org/10.1093/oxfordjournals.rpd.a006388
18. J. M. Gómez-Ros, R. Bedogni, D.A.V.I.D.E. Bortot, B. Buonomo, A. Esposito, A. Gentile, M. Lorenzoli, M.V. Introini, G. Mazitelli, M. Moraleda, A. Pola, D. Sacco, CYSP: A new cylindrical directional neutron spectrometer. Conceptual design. Radiat. Meas. 82, 47–51 (2015). https://doi.org/10.1016/j.radmeas.2015.07.005
19. R. Bedogni, J.M. Gómez-Ros, D. Bortot, A. Pola, M.V. Introini, A. Esposito, A. Gentile, G. Mazzitelli, B. Buonomo, Neutron spectrometry from thermal energies to GeV with single-moderator instruments. Eur. Phys. J. Plus **130**, 1–4 (2015). https://doi.org/10.1140/epjp/i2015-15024-6
20. N.T. Le, N.Q. Nguyen, H.Q. Nguyen, D.K. Pham, M.C. Nguyen, V.L. Bui, V.C. Cao, V.H. Duong, T.H. Duong, H.N. Tran, Cylindrical neutron spectrometer system: design and characterization. Eur. Phys. J. Plus **136**(6), 690 (2021). https://doi.org/10.1140/epjp/s13360-021-01681-9
21. R. Bedogni, A. Calamida, T. Napolitano, C. Cantone, A. M. Fontanilla, A. I. Castro Campoy, G. Abbatini, A. Pietropaolo, V. Monti, E. M. Mafucci, M. Bunce, D. Thomas, J.M. Gómez-Ros, S. Altieri, The NCT-WES directional neutron spectrometer: validation of the response with monoenergetic neutron fields. Eur. Phys. J. Plus, 138, 270 (2023). https://doi.org/10.1140/epjp/s13360-023-03840-6
22. R. Bedogni, A. Calamida, A. Fontanilla, A. I. Castro Campoy, T. Napolitano, C. Cantone, E. Mafucci, V. Monti, S. Altieri, J.M. Gómez-Ros, M. Pillon, A. Pietropaolo, Measuring the near-target neutron field of a D–D fusion facility with the novel NCT-WES spectrometer. Eur. Phys. J. Plus 137, 773 (2022). https://doi.org/10.1140/epjp/s13360-022-02922-1
23. Z.M. Hu, L.J. Ge, J.Q. Sun, Y.M. Zhang, T.F. Du, X.Y. Peng, J. Chen, H. Zhang, M. Nocente, M. Rebai, G. Croci, L.Q. Hu, G.Q. Zhong, R.J. Zhou, J.X. Chen, X.Q. Li, T.S. Fan, An active Bonner sphere spectrometer capable of intense neutron field measurement. Appl. Phys. Lett. **114**(23), 233502 (2019). https://doi.org/10.1063/1.5096191
24. J.G. Williams, D.M. Gilliam, Thermal neutron standards. Metrologia **48**(6), S254 (2011). https://doi.org/10.1088/0026-1394/48/6/S03
25. D.A. Brown, M.B. Chadwick, R. Capote, A.C. Kahler, A. Trkov, M.W. Herman, A.A. Sonzogni, Y. Danon, A.D. Carlson, M. Dunn, D.L. Smith, G.M. Hale, G. Arbanas, R. Arcilla, C.R. Bates, B. Beck, B. Becker, F. Brown, R.J. Casperson, J. Conlin, D.E. Cullen, M.-A. Descalle, R. Firestone, T. Gaines, K.H. Guber, A.I. Hawari, J. Holmes, T.D. Johnson, T. Kawano, B.C. Kiedrowski, A.J. Koning, S. Kopecky, L. Leal, J.P. Lestone, C. Lubitz, J.I. Márquez Dámian, C.M. Mattoon, E.A. McCutchan, S. Mughabghab, P. Navratil, D. Neudecker, G.P.A. Nobre, G. Noguere, M. Paris, M.T. Pigni, A.J. Plompen, B.Pritychenko, V.G. Pronyaev, D. Roubtsov, D. Rochman, P. Romano, P. Schillebeeckx, S. Simakov, M. Sin, I. Sirakov, B. Sleaford, V. Sobes, E.S. Soukhovitskii, I. Stetcu, P. Talou, I. Thompson, S. van der Marck, L. Welser-Sherrill, D. Wiarda, M. White, J.L. Wormald, R.Q. Wright, M. Zerkle, G. Žerovnik, Y. Zhu, ENDF/B-VIII. 0: the 8th major release of the nuclear reaction data library with CIELO-project cross sections, new standards and thermal scattering data. Nucl. Data Sheets 148, 1–142 (2018). https://doi.org/10.1016/j.nds.2018.02.001
26. Z.M. Hu, Y.H. Zheng, T.S. Fan, Z.Q. Cui, J. Chen, H. Zhang, G. Gorini, Q. Zhao, Experimental evaluation of the Geant4-calculated response functions of a Bonner sphere spectrometer on monoenergetic neutron sources. Nucl. Instrum. Methods Phys. Res. A **965**, 163836 (2020). https://doi.org/10.1016/j.nima.2020.163836
27. A. Fontanilla, A. Calamida, A. I. Castro Campoy, C. Cantone, A. Pietropaolo, J.M. Gómez-Ros, V. E. MontiMafucci, S. Vernetto, A. Pola, D. Bortot, R. Bedogni, Extended range Bonner sphere spectrometer for high-elevation neutron measurements. Eur. Phys. J. Plus 137, 1315 (2022). https://doi.org/10.1140/epjp/s13360-022-03439-3
28. L. Zhang, Y. Wang, H. Guo, C. Yu, H. Hu, Y. Liu, S. Chen, Transient current analysis of silicon carbide neutron detector using SRIM and TCAD. IEEE Sens. J. **22**(11), 10620–10629 (2022). https://doi.org/10.1109/JSEN.2022.3170570
29. T.M. Oakes, S.L. Bellinger, W.H. Miller, E.R. Myers, R.G. Fronk, B.W. Cooper, T.J. Sobering, P.R. Scott, P. Ugorowski, D.S. McGregor, J.K. Shultis, A.N. Caruso, An accurate and portable solid state neutron rem meter. Nucl. Instrum. Methods Phys. Res. A **719**, 6–12 (2013). https://doi.org/10.1016/j.nima.2013.03.060
30. H. Tagziria, D.J. Thomas, Calibration and Monte Carlo modelling of neutron long counters. Nucl. Instrum. Methods Phys. Res. A **452**(3), 470–483 (2000). https://doi.org/10.1016/S0168-9002(00)00448-4
31. Z.M. Hu, X.Y. Peng, Z.J. Chen, T.F. Du, L.J. Ge, X. Yuan, Z.Q. Cui, W.J. Zhu, Z.M. Wang, X. Zhu, J.X. Chen, X.Q. Li, G.H. Zhang, J. Chen, H. Zhang, G. Gorini, T.S. Fan, Experimental characterization of a long counter for neutron fluence measurement. Radiat. Meas. **119**, 16–21 (2018). https://doi.org/10.1016/j.radmeas.2018.08.017
32. M. Reginatto, Resolving power of a multisphere neutron spectrometer. Nucl. Instrum. Methods Phys. Res. A **480**(2–3), 690–695 (2002). https://doi.org/10.1016/S0168-9002(01)01207-4